JOURNAL OF SPACECRAFT AND ROCKETS
Vol. 31, No. 5, September–October 1994

Three-Dimensional Structure of a Supersonic Jet Impinging on an Inclined Plate

Kyoung-Ho Kim* and Keun-Shik Chang†
Korea Advanced Institute of Science and Technology, Taejon 305-701, Republic of Korea

The flow structure of an underexpanded supersonic jet impinging on an inclined flat plate has been numerically investigated using a total-variation-diminishing scheme for the Euler equations. The impinging jet is characterized by many discontinuities, such as barrel shock, exhaust gas jet boundary, Mach disk, reflected shock, plate shock, subtail shock, contact surface, and sometimes a stagnation bubble. Furthermore, if the plate is inclined, the jet structure becomes three-dimensional and severely distorted. The effect of plate inclination has been investigated in the present paper by studying the formation of the asymmetric stagnation bubble and the magnitude and location of the maximum wall pressure. Comparison with the existing experimental results over a broad range of data sets on pressure and shock structure has led to the conclusion that the present inviscid numerical model can offer fairly good prediction of the impinging jet for moderate plate inclinations. The maximum wall pressure was found to be larger on the inclined plate than on the normal plate.

Nomenclature

A_k = Jacobian matrix, $k = \xi, \eta, \zeta$
D_n = nozzle-exit diameter
e = total internal energy per unit volume
F, G, H = flux vectors in general curviliner coordinates
J = metric Jacobian
L_k = operator, $k = \xi, \eta, \zeta$
M = matrix of transformation between conservative and primitive variables
P, p = pressure
Q = conservative state vector
t = time
T_k = transformation matrix, $k = \xi, \eta, \zeta$
u, v, w = velocity components in Cartesian coordinates
X_{np} = nozzle-to-plate spacing
x, y, z = Cartesian coordinates
Δ = difference
γ = specific heat ratio
λ_k = $\Delta\tau/\Delta k$, $k = \xi, \eta, \zeta$
Λ_k = diagonal matrix, $k = \xi, \eta, \zeta$
ρ = density
θ = plate inclination angle
τ = time
ξ, η, ζ = general coordinates

Subscripts
amb = ambient condition
jet = jet condition
n = nozzle

Superscripts
N = numerical flux
n = original flux
$\pm$ = split condition

Introduction

A SUPERSONIC jet impinging on a surface has broad application. Liftoff of V/STOL aircraft, missile launching systems, the muzzle brake of a gun, thrust vectoring of flight vehicles, multistage rocket separation, and deep-space docking are a few examples. An impinging jet has complicated flow elements consisting of barrel shock, exhaust gas jet boundary, Mach disk, contact surface, reflected shock, plate shock, subtail shock, and sometimes a stagnation bubble. The jet will be axisymmetric in free expansion or in normal impingement, but will become three-dimensional when the jet impinges on an inclined surface.

In the past, many experimental[1–4] and numerical[5–8] investigations have been performed to study the impinging process of a supersonic jet. Previous work in this area has mainly concentrated on perpendicular plates, which arise in a wide variety of the situations mentioned above. One of the phenomena to attract interest was the occurrence of a stagnation bubble attached to the plate, which is known to play a vital role in the shock-wave instability of an impinging jet.[8] The mechanism and criterion for formation of a stagnation bubble was studied in Ref. 1. Studies of jet flow parameters included the effect of jet exit pressure in Refs. 2 and 3; the effect of nozzle-to-plate spacing in Refs. 1, 2, 3, 5, and 6; the impingement of a high-enthalpy jet in Ref. 7; and the shock-wave instability associated with the fluctuating stagnation bubble in Ref. 8. However, the structure of a three-dimensional jet and its deformation with respect to the plate inclination angle has not been theoretically explored so far, although Ref. 3 conducted experimental studies, providing a series of shadowgraphs and measurements. In this paper, the underexpanded supersonic jet impinging on an inclined flat plate has been numerically investigated using a total-variation-diminishing (TVD) scheme for the Euler equations. The extreme directional bias of the flowfield would not allow any central difference scheme with artificial viscosity to be utilized; in addition these schemes also cause difficulty in implementing the boundary conditions. The TVD scheme employed here uses the modified flux approach[9] and symmetric dimensional splitting for the flux derivatives. This TVD scheme is completely defined in the sense that the user does not have to specify any numerical parameter or dissipation coefficient to achieve stability, contrary to the conventional central difference schemes.

Euler Equations and Numerical Algorithm

The conservation-form three-dimensional Euler equations of gasdynamics in the general curvilinear coordinate system (τ, ξ, η, ζ) are employed,

$$\partial_\tau Q + \partial_\xi F + \partial_\eta G + \partial_\zeta H = 0 \tag{1}$$

The flux vectors are defined by

$$\begin{aligned} Q &= \bar{Q}/J \\ F &= (\xi_t \bar{Q} + \xi_x \bar{F} + \xi_y \bar{G} + \xi_z \bar{H})/J \\ G &= (\eta_t \bar{Q} + \eta_x \bar{F} + \eta_y \bar{G} + \eta_z \bar{H})/J \\ H &= (\zeta_t \bar{Q} + \zeta_x \bar{F} + \zeta_y \bar{G} + \zeta_z \bar{H})/J \end{aligned} \tag{2}$$

Received Feb. 16, 1993; revision received Oct. 6, 1993; accepted for publication Nov. 24, 1993.
*Research Engineer, Hyundai Motor Company.
†Professor, Department of Aerospace Engineering. Member AIAA.

Here, a bar on a quantity implies that it is either a state vector or a flux vector in the Cartesian coordinate system (t, x, y, z), and J is the metric Jacobian

$$J^{-1} = (x_\xi y_\eta - x_\eta y_\xi)z_\zeta + (x_\zeta y_\xi - x_\xi y_\zeta)z_\eta + (x_\eta y_\zeta - x_\zeta y_\eta)z_\xi \quad (3)$$

For an ideal gas we add the equation of state

$$p = (\gamma - 1)[e - \rho(u^2 + v^2 + w^2)/2] \quad (4)$$

Similarity transformation is made on the Jacobian matrices A_k $(k = \xi, \eta, \zeta)$ using the transformation matrix T_k, defined by

$$T_k^{-1} M^{-1} A_k M T_k = \Lambda_k, \qquad k = \xi, \eta, \zeta \quad (5)$$

where $M = \partial \bar{Q}/\partial \bar{Q}^p$ is the matrix of transformation between the conservative variables $\bar{Q}$ and the primitive variables $\bar{Q}^p = [\rho, u, v, w, p]^T$. The diagonal matrix is given by

$$\Lambda_k = \text{diag}\{a_{k_m}\} \quad (6)$$

where a_{k_m} $(k = \xi, \eta, \zeta$ and $m = 1, 2, \ldots, 5)$ are the eigenvalues of the Jacobian matrix A_k.

Extending the explicit characteristic flux-difference splitting method used in two dimensions,[10] we obtain

$$\partial_\tau Q + (A_\xi^+ + A_\xi^-)\partial_\xi F + (A_\eta^+ + A_\eta^-)\partial_\eta G + (A_\zeta^+ + A_\zeta^-)\partial_\zeta H = 0 \quad (7)$$

where the normalized Jacobian coefficient matrices can be defined as before:

$$A_k^\pm = M T_k \Lambda_k^\pm T_k^{-1} M^{-1}, \qquad k = \xi, \eta, \zeta \quad (8)$$

with

$$\Lambda_k^\pm = \text{diag}\{a_{k_m}^\pm\} \quad (9)$$

where

$$a_{k_m}^\pm = \frac{1 \pm \text{sign}\,(a_{k_m})}{2}, \qquad k = \xi, \eta, \zeta, \quad m = 1, 2, \ldots, 5 \quad (10)$$

To solve Eq. (7), explicit time-differencing is employed with symmetric locally one-dimensional operator splitting as

$$Q_{i,j,k}^{n+2} = L_\xi L_\eta L_\zeta L_\zeta L_\eta L_\xi (\Delta\tau) Q_{i,j,k}^n \quad (11)$$

For the operator L_ξ in the ξ direction, for example, we use the definition

$$L_\xi Q_{i,j,k}^n = Q_{i,j,k}^n - \lambda_\xi \left(F^N_{i+\frac{1}{2},j,k} - F^N_{i-\frac{1}{2},j,k} \right) \equiv Q^*_{i,j,k} \quad (12)$$

where $\lambda_\xi = \Delta\tau/\Delta\xi$ and the numerical flux F^N is given by

$$F^N_{i+\frac{1}{2},j,k} = F^n_{i+1,j,k} - (\Delta F)^+_{i+\frac{1}{2},j,k} \quad (13)$$

with

$$(\Delta F)^\pm_{i+\frac{1}{2},j,k} = A^\pm_{\xi\, i+\frac{1}{2},j,k} \Delta_{i+\frac{1}{2},j,k} F^n$$

$$= A^\pm_{\xi\, i+\frac{1}{2},j,k} \left(F^n_{i+1,j,k} - F^n_{i,j,k} \right) \quad (14)$$

Numerical stability limits the size of time step to

$$\Delta\tau = \text{CFLN} \min[\Delta k / \max(a_{k_m});\ k = \xi, \eta, \zeta,\ m = 1, 2, \ldots, 5] \quad (15)$$

where CFLN is the Courant-Friedrichs-Lewy number.

To retain the second-order accuracy for the convection terms and to make the total variation stable, a modified flux vector is used in place of the original flux, following Ref. 9. Further detail may be found in Refs. 7 and 8.

Boundary Conditions

For the flat plate the predicted solution that is obtained with one-sided sweeping, Q^*, is supplied to the Riemann invariants corresponding to the local characteristics and to the surface tangency condition. More detailed description of the boundary conditions may be found in Refs. 7, 8, 10, and 11.

A similar procedure is applicable to the other boundaries: the vertical symmetry plane that halves the computational domain, and the far boundary.

Results and Discussion

The impinging jet under investigation is assumed to have following parameter values: $M_{\text{jet}} = 2.2$, PR $(= P_{\text{jet}}/P_{\text{amb}}) = 1.2$, $X_{\text{np}} = 3D_n$, and varied plate inclination angles $\theta = 45$ to 90 deg. Here M_{jet} is the flow Mach number at the nozzle exit, and X_{np} is the nozzle-to-plate spacing measured along the geometric jet axis. The reference pressure and temperature are, respectively, $P_{\text{amb}} = 1$ atm and $\rho_{\text{amb}} = 1.225$ kg/m^3. Figure 1 depicts the physical domain of the impinging jet flow. Cartesian coordinates were used, with the number of grid points $46 \times 56 \times 31$.

Initial jet flow data required at the nozzle exit were provided by solving a priori a nozzle problem: a converging-diverging nozzle having a conical diverging section of 15-deg semiangle. The Sauer method[12] was adopted for the initial conditions, and the method of characteristics for the flowfield computation.

The complex flow structures of an underexpanded supersonic jet impinging on a plate, such as the properties discussed in the Introduction, all significantly depend on such flow parameters as jet exit pressure, reservoir temperature, nozzle-to-plate spacing, and plate inclination angle. The characteristic features of jet structure related to the nozzle-to-plate spacing, the reservoir temperature, and shock-wave instability have been investigated in sufficient detail in companion papers by the present authors.[6-8] When the jet flow impinges on an inclined plate, the flowfield becomes severely distorted from the pattern exhibited by the jet impinging on a normal plate. The position and magnitude of the maximum wall pressure and near-wall temperature change as the plate and plate shock are inclined. The stagnation bubble, if it exists, may collapse, depending upon the plate inclination angle.

Axisymmetric Jet Impingement, $\theta = 90$ deg

Figure 2 shows the schemetic sketch of the impinging jet flow, illustrating all the complicated flow elements mentioned earlier except the stagnation bubble. Figure 3 presents the computed density contours for $\theta = 90$ deg. The structure of a jet impinging on a plate clearly includes the barrel shock, (exhaust gas) jet boundary, Mach disk, reflected shock, plate shock, subtail shock, and contact surface. The wall pressure distribution along the line of symmetry on the plate is presented in Fig. 4, where comparison is made between

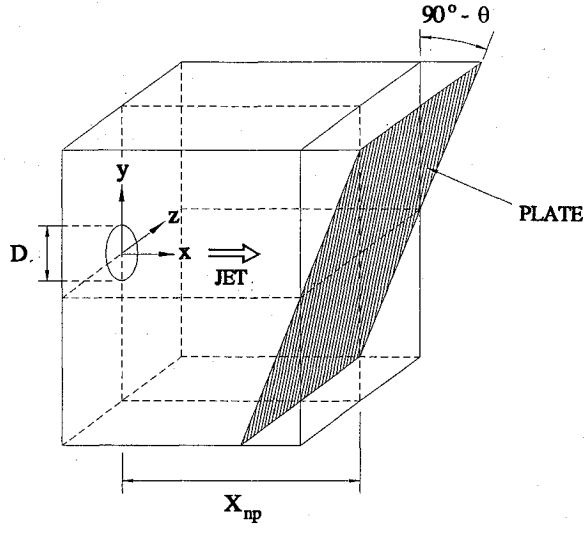

Fig. 1 Flowfield geometry.

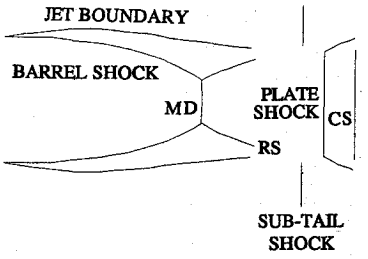

Fig. 2 Schematic sketch of the impinging jet: CS, contact surface; MD, Mach disk; RS, reflected shock.

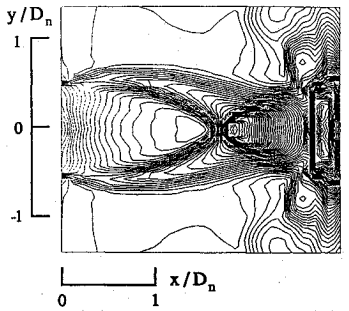

Fig. 3 Density contours in the x-y plane at $z = 0$ for $\theta = 90$ deg; $\rho_{min}/\rho_\infty = 0.30$, $\rho_{max}/\rho_\infty = 7.64$, $\Delta\rho/\rho_\infty = 0.1$.

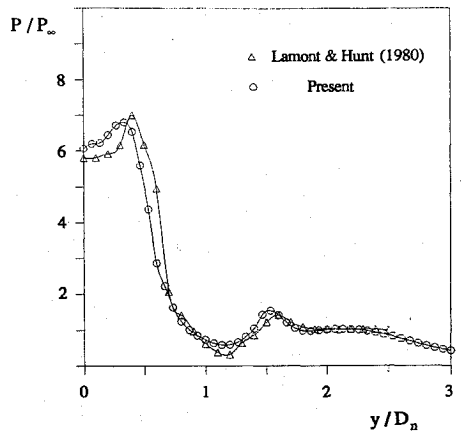

Fig. 4 Comparison of wall pressure along the line of symmetry for $\theta = 90$ deg.

the experiment[3] and the present computation. In the experiment the maximum pressure, 6.99 atm, occurs at the position $y = 0.40D_n$, which represents the ring-shaped stagnation line at the boundary of the stagnation bubble, whereas its computational counterpart has maximum pressure 6.79 atm at $y = 0.33D_n$ (see also Table 1). The relative error for the maximum wall pressure is 2.9% in this case, and its predicted position is in fair agreement with the experiment.[3] The computed recompression shock occurs approximately between $y = 1.5D_n$ and $1.6D_n$, which is again in good agreement with the experiment.

$\theta = 85$-deg Impingement

Figure 5 shows the density contours in the plane of symmetry, the x-y plane at $z = 0$ (see Fig. 1), which indicate the plate shock is slanted. The flow field in the x-z plane at $y = 0$ is shown in Fig. 6, where similarity with the axisymmetric case, $\theta = 90$ deg, is evident. The isobars on the inclined flat plate are given in Fig. 7. Some flow peculiarites are indicated: first, the major flow expansion occurs just outside of the boundary of the central region containing the stagnation bubble, where the isobars are densely clustered, and second, we can estimate the size of the recompression shock wave, with an approximately circular ring shape, which separates the expanding supersonic jet flow from the outside subsonic flow. The shapes and strengths of the high-pressure central region and the recompression shock wave will be the important data sought for designing a missile launcher system.

Table 1 Maximum pressure on the plate as a function of the plate inclination

Plate inclination angle, deg	E_{max}, atm		
	Expt.[3]	Calc.	Rel. error, %
90	6.99	6.79	2.9
85	8.60	7.81	9.2
80	9.88	8.97	9.1
70	8.47	7.65	9.7
60	8.34	7.48	10.3
45	8.85	6.40	27.7

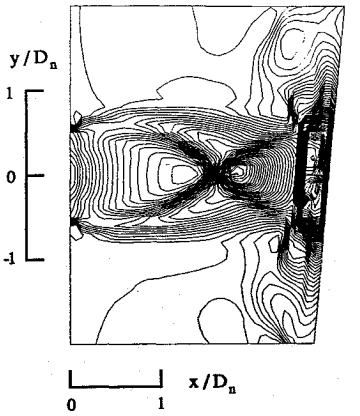

Fig. 5 Density contours in the x-y plane at $z = 0$ for $\theta = 85$ deg; $\rho_{min}/\rho_\infty = 0.28$, $\rho_{max}/\rho_\infty = 7.45$, $\Delta\rho/\rho_\infty = 0.1$.

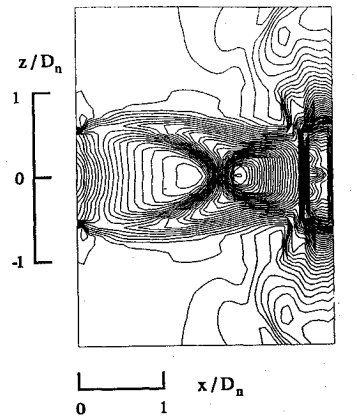

Fig. 6 Density contours in the x-z plane at $y = 0$ for $\theta = 85$ deg; $\rho_{min}/\rho_\infty = 0.32$, $\rho_{max}/\rho_\infty = 6.79$, $\Delta\rho/\rho_\infty = 0.1$.

Figure 8 presents for $\theta = 85$ deg the wall pressure distribution along the line of symmetry on the plate. The computed peak pressures and their positions are in close agreement with those from the experiment.[3] The pressure distribution reveals existence of a stagnation bubble (see also Figs. 9–11), contrary to the case $\theta = 90$ deg, which is characterized by a small portion of horizontal curve or trough between the local peak pressures near the central axis. The computed maximum wall pressure increased from 6.79 atm at the angle $\theta = 90$ deg to 7.81 atm at $\theta = 85$ deg, whereas the maximum wall pressure in the experiment[3] showed an increase from 6.99 atm at $\theta = 90$ deg to 8.60 atm at $\theta = 85$ deg. The increase of maximum wall pressure due to the plate inclination is closely related to the three-dimensional shape of the slanted plate shock (see also Fig. 5), which manifests reduced total pressure loss across the shock-wave surface. The relative error for the maximum wall pressure along the line of symmetry between the computation and the experiment[3] is about 9% at $\theta = 85$ deg, and the position of peak pressure is also in close agreement with the experiment.

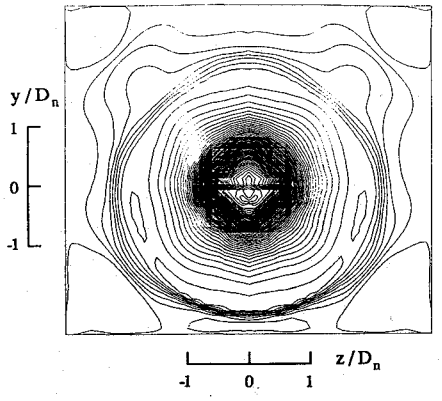

Fig. 7 Isobars on the flat plate for $\theta = 85$ deg; $P_{min}/P_\infty = 0.13$, $P_{max}/P_\infty = 7.81$, $\Delta P/P_\infty = 0.1$.

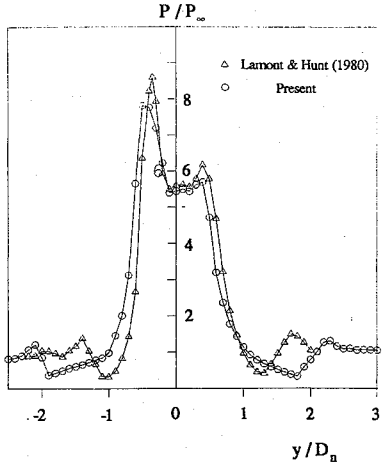

Fig. 8 Comparison of wall pressure along the line of symmetry for $\theta = 85$ deg.

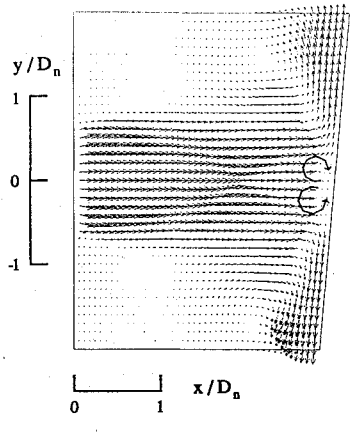

Fig. 9 Velocity vector plots in the x-y plane at $z = 0$ for $\theta = 85$ deg.

Figures 9–11 show the velocity vector plots where a recirculating flow region or stagnation bubble is observed in the form of a small hemispherical region attached to the plate. The pattern of surface flow on the plate is shown in Fig. 11 by the velocity vectors. It is observed that a dividing ring, designated by a solid line (the stagnation line as well as the boundary of stagnation bubble), separates the radially expanding flow from the stagnation bubble directed radially inward on the flat plate. This flow pattern was explained in Ref. 4. The stagnation bubble contains relatively slowly moving fluid and forms a high-pressure region having the local peak pressure at its boundary.

$\theta = 80$ deg Impingement

Figure 12 represents the density contours in the x-y plane at $z = 0$, which shows that the plate shock is more slanted. The flowfield in the x-z plane at $y = 0$ is shown in Fig. 13, which has flow

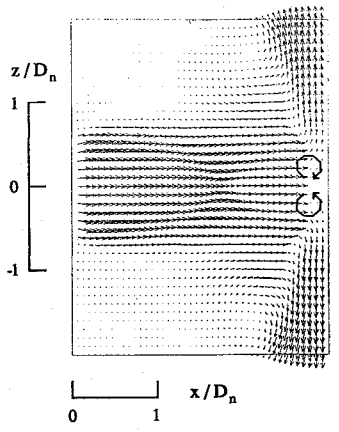

Fig. 10 Velocity vector plots in the x-z plane at $y = 0$ for $\theta = 85$ deg.

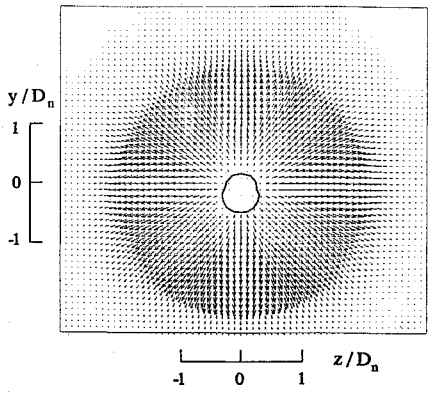

Fig. 11 Velocity vector plots on the flat plate for $\theta = 85$ deg.

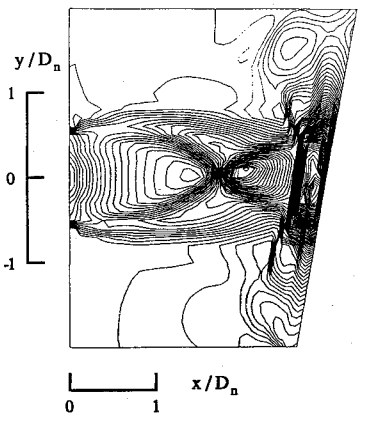

Fig. 12 Density contours in the x-y plane at $z = 0$ for $\theta = 80$ deg; $\rho_{min}/\rho_\infty = 0.28$, $\rho_{max}/\rho_\infty = 8.48$, $\Delta_\rho/\rho_\infty = 0.1$.

patterns about the same as for $\theta = 90$ deg (axisymmetric jet) and $\theta = 85$ deg, meaning that the flowfield in the x-z plane is nearly independent of the plate inclination. The isobars on the slanted flat plate are given in Fig. 14.

The wall pressure distribution along the line of symmetry on the plate is presented in Fig. 15. The computed maximum pressure increased from 7.81 atm at $\theta = 85$ deg to 8.97 atm at $\theta = 80$ deg, whereas their experimental values[3] changed from 8.60 atm at $\theta = 85$ deg to 9.88 atm at $\theta = 80$ deg, corresponding to about 9% relative error. The single-peaked central hump in the central region of the pressure curve of Fig. 15 also indicates that the bubble has now collapsed. This fact can be also confirmed by plotting the velocity vectors (not presented here). This result is consistent with the earlier experiment,[3] which reported that the stagnation bubble exists only for $\theta \geq 85$ deg. Calculations have been obtained for the cases $\theta = 70, 60$, and 45 deg; these results are not presented here for reasons of space. It is noted, however, that the results were similar to the case for $\theta = 80$ deg.

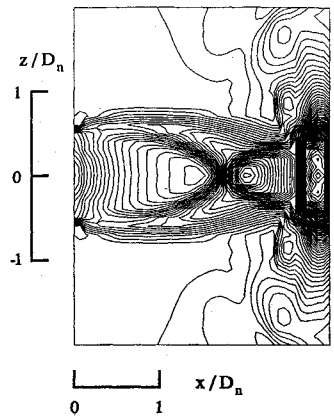

Fig. 13 Density contours in the x-z plane at $y = 0$ for $\theta = 80$ deg; $\rho_{min}/\rho_\infty = 0.32$, $\rho_{max}/\rho_\infty = 8.04$, $\Delta_\rho/\rho_\infty = 0.1$.

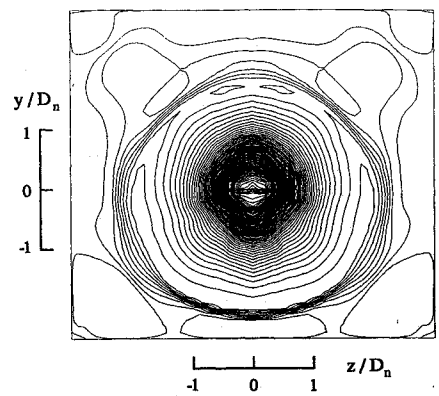

Fig. 14 Isobars on the flat plate for $\theta = 80$ deg; $P_{min}/P_\infty = 0.11$, $P_{max}/P_\infty = 8.97$, $\Delta_P/P_\infty = 0.1$.

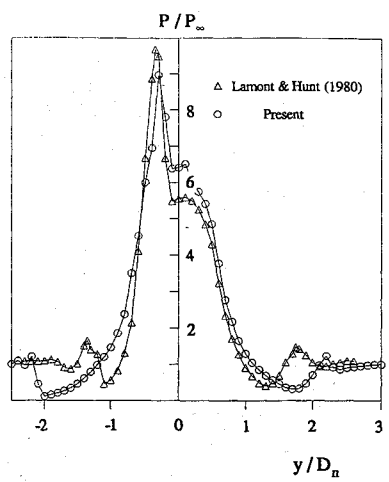

Fig. 15 Comparison of wall pressure along the line of symmetry for $\theta = 80$ deg.

Table 1 summarizes the maximum wall pressures for both the experiment[3] and the present computation, and their relative errors. The change in the maximum wall pressure with plate inclination angle from the computation is clearly consistent with that of the experiment.[3] The maximum wall pressure increases very sharply at first when the plate is inclined from $\theta = 90$ deg to 80 deg, because the total pressure loss is decreased by the slanted plate shock surface. As the plate is further inclined beyond $\theta = 80$ deg, however, the maximum pressure slightly decreases. This may be due to restructuring of the lower part of the plate shock, exemplified by the occurrence of an inner triple point as shown by Lamont and Hunt.[3] It is noted that the relative error remains within 10% except for the case of an extreme inclination angle, $\theta = 45$ deg. This implies that the present numerical method is a reasonable engineering tool for analysis of the supersonic jet impinging on an inclined plate.

Conclusion

The flowfield generated by a supersonic jet impinging on an inclined plate has been numerically simulated by using a TVD scheme for the inviscid compressible Euler equations. The computed three-dimensional jet flow produced results comparable to the experimental result of Lamont and Hunt[3] for moderate plate inclinations. The stagnation bubble may or may not exist, depending on the plate inclination angle; the bubble existing at $\theta = 85$ deg disappeared when the plate was inclined further to $\theta = 80$ deg and beyond. The maximum wall pressure on the inclined plates exceeds that on a perpendicular plate. The jet structure, however, stays nearly constant in the x-z plane, independent of the plate inclinations. The flow information obtained in this paper, such as density contours, isobars, velocity vectors, and wall pressure distribution along the line of symmetry on the plate, has been very effective in determining the structure of impinging jets.

References

[1]Kalghatgi, G. T., and Hunt, B. L., "Occurrence of Stagnation Bubble in Supersonic Jet Impingement Flows," *The Aeronautical Quarterly*, Vol. 27, No. 3, Aug. 1976, pp. 169–185.

[2]Ginzburg, I. P., Semilentenco, B. G., Terpigorer, V. S., and Uskov, V. N., "Some Singularities of Supersonic Underexpanded Jet Interaction with a Plane Obstacle," *Journal of Engineering Physics*, Vol. 19, No. 3, 1970, pp. 1081–1084.

[3]Lamont, P. J., and Hunt, B. L., "The Impingement of Underexpanded, Axisymmetric Jets on Perpendicular and Inclined Flat Plate," *Journal of Fluid Mechanics*, Vol. 100, No. 3, 1980, pp. 471–511.

[4]Donaldson, C. duP., and Snedeker, R. S., "A Study of Free Jet Impingement. Part 1. Mean Property of Free and Impinging Jet," *Journal of Fluid Mechanics*, Vol. 45, No. 2, 1971, pp. 281–319.

[5]Iwamoto, J., "Impingement of Underexpanded Jets on a Flat Plate," *Journal of Fluid Engineering*, Vol. 112, No. 2, June 1990, pp. 179–184.

[6]Kim, K. H., and Chang, K. S., "Axisymmetric Jet Impingement on a Flat Plate: Numerical Simulation using a TVD Scheme," *Proceedings of the 18th International Symposium on Shock Waves*, edited by K. Takayama, Springer-Verlag, 1992, pp. 1069–1073.

[7]Kim, K. H., and Chang, K. S., "Axisymmetric Impingement of Hot Jet into a Flat Plate: Equilibrium Flow Analysis of High Temperature Air," *Shock Waves, an International Journal* (to be published).

[8]Kim, K. H., "Numerical Analysis of Supersonic Jets Impinging into an Obstacle," Ph.D. Dissertation, KAIST, Taejon, Korea, Aug. 1993.

[9]Harten, A., "High Resolution Schemes for Hyperbolic Conservation Laws," *Journal of Computational Physics*, Vol. 49, No. 3, 1983, pp. 357–393.

[10]Yang, J. Y., Lombard, C. K., and Bershader, D., "Numerical Simulation of Transient Inviscid Shock Tube Flows," *AIAA Journal*, Vol. 25, No. 2, 1987, pp. 245–251.

[11]Osher, S., and Chakravarthy S., "Upwind Scheme and Boundary Conditions with Application to Euler Equations in General Geometries," *Journal of Computational Physics*, Vol. 50, No. 3, 1983, pp. 447–481.

[12]Zucrow, M. J., and Hoffman, J. D., *Gas Dynamics*, Vol. II, Wiley, New York, 1977, pp. 86–110.